Supporting Information

High-Fidelity Self-Assembly of Crystalline and Parallel-Oriented Organic Thin Films by π–π Stacking from a Metal Surface

Daniel Skomski,[1] Junyong Jo,[1] Christopher D. Tempas,[1] Seyong Kim,[2] Dongwhan Lee,*[,2] and Steven L. Tait*[,1]

1 Department of Chemistry, Indiana University, Bloomington, IN 47405, United States

2 Department of Chemistry, Seoul National University, Gwanak-ro 1, Seoul 151-747, Republic of Korea

E-mail: tait@indiana.edu; dongwhan@snu.ac.kr

Contents

Section S1. Synthesis of TPT

The synthesis of tris(*N*-phenyltriazole) (TPT; 2,5,8-triphenyl-benzo[1,2-*d*:3,4-*d*':5,6-*d*"]tris([1,2,3]triazole) was initially reported by Muzik and Allan,[1] but without any detailed experimental procedures or spectroscopic data provided for either the synthetic intermediate or the final product. We thus report optimized synthetic protocols, and spectroscopic (^{1}H/^{13}C NMR; IR) and mass spectrometric data for each.

*2,4,6-Tris((E)-phenyldiazenyl)benzene-1,3,5-triamine***.** A flask (50 mL) was charged with aniline (392 mg, 4.21 mmol), conc. HCl (1.50 mL), MeOH (15 mL), and a magnetic stir bar and cooled to 0 °C. A pre-cooled (0 °C) aq solution (5 mL) of $NaNO_2$ (353 mg, 5.12 mmol) was delivered using a pipet over a period of 10 min, and the reaction mixture was stirred for additional 10 min at 0 °C. A 250 mL round-bottom flask was charged with 1,3,5-triaminobenzene (129 mg, 1.05 mmol), MeOH (20 mL), and pyridine (5 mL), and cooled to 0 °C. A pipet was used to deliver the diazonium reaction mixture of aniline over a period of 10 min. The resulting mixture was stirred for additional 20 min at 0 °C. Addition of water (200 mL) induced precipitation of a bright orange solid, which was isolated by filtration and washed with water several times. The orange solid (432 mg, 0.993 mmol, yield = 94.8%) was dried in air. ^{1}H NMR (400 MHz, $CDCl_3$, 298 K). δ 7.67–7.60 (d, J = 7.4 Hz, 6H), 7.44–7.48 (t, J = 7.4 Hz, 6H), 7.32–7.34 (t, J = 7.0 Hz, 3H). ^{13}C NMR (100 MHz, $CDCl_3$, 298 K) 153.2, 129.1, 127.9, 121.0. FT-IR (KBr pallet, cm^{-1}): 3503, 3430, 3383, 3161, 1573, 1518, 1454, 1351, 1309, 1241, 1200, 1117, 911, 761, 686, 593, 506, 475, 448, 419. HRMS (ESI). calcd for $C_{24}H_{22}N_9$ $[M + H]^+$ 436.1998, found 436.2002.

*2,5,8-Triphenyl-benzo[1,2-d:3,4-d':5,6-d'']tris([1,2,3]triazole) (TPT)***.** A flask (100 mL) was charged with 2,4,6-tris((*E*)-phenyldiazenyl)benzene-1,3,5-triamine (496 mg, 1.14 mmol), pyridine (35 mL), and $Cu(OAc)_2{\cdot}H_2O$ (2.21 g, 11.1 mmol). The reaction mixture was heated at reflux for 30 min. After cooling to r.t., water (60 mL) was added to induce precipitation of a white solid, which was isolated by filtration and washed with excess amount of water and MeOH (5 mL). The white solid material was dried in the air to afford **TPT** (568 mg, 1.32 mmol, yield = 90.4%). ^{1}H NMR (400 MHz, $CDCl_3$, 298 K). δ 8.47–8.49 (d, J = 8.2 Hz, 6H), 7.59–7.63 (d, J = 7.8 Hz, 6H), 7.49–7.51 (d, J = 2.0 Hz, 3H). ^{13}C NMR (100 MHz, $CDCl_3$, 298 K): δ 139.9, 137.2, 129.5, 128.8, 120.0. FT-IR (KBr pallet, cm^{-1}): 3432, 3063, 2819, 2401, 2361, 1977, 1946, 1624, 1596, 1497, 1463, 1369, 1336, 1312, 1298, 1165, 1075, 1024, 962, 917, 751, 685, 663, 649, 530, 493. HRMS (ESI). calcd for $C2_4H_{16}N_9$ $[M + H]^+$ 430.1529, found 430.1548.

Section S2. Fabrication and Characterization of TPT Films in Ultra-high Vacuum

Experiments were conducted in an ultra-high vacuum (UHV) system of base pressure $< 5 \times 10^{-10}$ Torr. The silver (111) and gold (100) single crystal surfaces (Princeton Scientific Corp.) were each cleaned by cycles of argon ion sputtering at a sample temperature of 200 °C and thermal annealing to 480–500 °C. XPS analysis of the C 1*s* and N 1*s* regions, as well as STM/NC-AFM imaging, were used to verify surface cleanliness. TPT was deposited from a quartz-lined, Knudsen-type evaporator at a crucible temperature of 215–235 °C after degassing for many hours at 120–180 °C. A mechanical shutter was used to regulate the film thickness.

The experimental data presented in the manuscript were acquired from several separate sample preparations. The sample in Figure 4a was prepared by depositing 3.2 ± 0.7 ML onto the Ag(111) surface at room temperature. That sample was then annealed at 150 °C to produce the monolayer sample shown in Figure 1a (overlayers desorb at 150 °C, leaving behind a well-ordered monolayer). Then, more TPT was deposited at room temperature to raise the surface coverage to 1.4 ML (Figure 1c and 1d). In a second experiment, starting from clean Ag(111), TPT was deposited at room temperature to produce the monolayer sample in Figure 5a, then subsequent deposition to 3.8 ± 0.8 ML (STM image in Figure 4b, NC-AFM image in 4c), then annealed at 45 °C, and another deposition to bring the total coverage to 6.1 ± 1.3 ML (Figures 1e, 1f, and 4d). Further deposition on the same sample was carried out to bring the total coverage to 14 ± 4 ML (STM image in Figure 4e, photograph in Figure 4g). In a third experiment, deposition was done to > 20 ML at room temperature (Figure 4f). In a fourth experiment, a single monolayer was deposited with the sample held at 50 °C during the deposition (Figure 5d). In a fifth experiment, deposition to 8.9 ± 2.1 ML was done with the sample held at 50 °C during the deposition (Figure 5e). In a sixth experiment, deposition to a coverage comparable to the sample in Figure 5e was done at room temperature (Figure 5b). The data presented for growth on the Au(100) surface are from two separate experiments, each starting from the clean, reconstructed Au(100) surface with growth at room temperature to 1.25 ML (Figure 6a) or 3.2 ML (Figures 6c and 6e).

The dual STM/NC-AFM microscope (RHK Technologies SPM UHV 750) was operated at room temperature to obtain topographic images of the surface. Calibration of the microscope was performed via images of the well-characterized (3×3) structure of terephthalic acid on the Cu(100) surface.[2] Sharp tungsten STM tips were fabricated via electrochemical etching. Bias voltages of 0.8 V to 1.4 V and set point currents from 0.2 nA to 0.5 nA were used in STM imaging. The AFM was operated in non-contact mode with antimony-doped single crystal silicon

cantilevers (NSG10, NT-MDT Co., f_0 = 280 kHz) and frequency shift setpoints of 18–20 Hz. STM and NC-AFM image analysis was carried out with the WSxM software.[3]

A commercial energy analyzer (PHOIBOS 150, SPECS GmbH) and dual anode Mg/Al X-ray source (XR-50, SPECS GmbH) were used for all XPS experiments. Spectral analysis was conducted with the SpecsLab2 and CasaXPS software. Linear background subtraction and corrections for the transmission factor, the mean free path of the electrons, and relative sensitivity factors were applied to the XPS photoelectron peaks. XPS peak positions were corrected for the work function of the energy analyzer via the Ag $3d_{5/2}$ binding energy of the atomically-clean Ag surface (368.3 eV).[4] XPS peak intensities were calculated as ratios to the Ag $3d_{5/2}$ peak area of the atomically-clean Ag surface to account for changes in detector sensitivity. XPS spectral analysis of the TPT films showed only features corresponding to carbon, nitrogen, and either silver or gold; *i.e.*, the films are chemically pure.

Section S3. Quantification of TPT Surface Coverage

To determine the TPT surface coverage, the XPS C 1*s* signal intensity was correlated to the number of atomic layers with Eqn. S1.[5] In this equation, I_x is the total XPS C 1*s* intensity of the multilayer film with a surface coverage of *x* molecular layers, λ is the mean free path length of the C 1*s* electrons in the sample, *z* is the molecular inter-layer spacing, and $I_{saturation}$ is the XPS C 1*s* intensity when the TPT film is sufficiently thick to saturate the C 1*s* photoemission signal. Atomically clean metal samples were used to correct for changes in the detector sensitivity between the XPS experiments. The film growth mode was experimentally determined to be Frank-van der Merwe (layer-by-layer) from micrometer-scale NC-AFM images. Furthermore, STM/NC-AFM images showed that the multilayers were well-ordered and maintained the same 2D packing as the monolayer. The interlayer separation between the parallel-displaced TPT molecules was experimentally determined from non-contact AFM topographic height profiles of the organic multilayers (z = 3.2 ± 0.2 Å). The XPS C 1*s* signal intensity of the monolayer (red dot in Figure S2; $I_{monolayer}$ = 2,744.3 ± 54.9 CPS·eV) is known from comparison to STM/NC-AFM experiments. Scanning probe microscopy can identify the transitions from sub-monolayer to complete monolayer to more than one monolayer, and thereby allows for accurate calibration to XPS intensity. The XPS intensity for 1.0 ML was carefully calibrated to multiple STM and NC-AFM experiments with TPT and with terephthalic acid,[2, 6-8] a compound whose monolayer has been well characterized by our group and by other groups. Furthermore, annealing of the multilayer structure at 150 °C for 15 min induces desorption of the multilayer, but does not desorb the monolayer as confirmed by STM/NC-AFM, thereby enabling another means to determine the exact monolayer photoemission intensity. To determine the saturation intensity, the experimental XPS C 1*s* intensity was plotted versus the TPT deposition time (Figure S1). Three consecutive depositions onto the same sample (blue dots in Figure S1; total deposition time >10 h) yielded the same sample C 1*s* intensity; *i.e.*, TPT material was depositing to the surface but the photoemission signal was saturated ($I_{saturation}$ = 17,350.9 ± 601.1 CPS·eV). The signal saturation is indicated by the blue lines in Figures S1 and S2. The general formula for the attenuation of the photoemission intensity of a single molecular layer, with electrons traversing an overlayer material of thickness *d*, is given in Eqn. S2. The total photoemission intensity of the film is thus the summation of the attenuated intensities of the different molecular layers (Eqn. S3). The mean free path length of the electrons was calculated from Eqn. S3 (λ = 20.2 ± 2.5 Å). The plot in Figure S2 was generated by fitting Eqn. S1 to the known monolayer XPS intensity and the known

value of the signal saturation. That function was then used to determine other film thicknesses (black dots in Figure S2) with the 3.2 Å interlayer spacing determined from NC-AFM.

$$I_x = I_{saturation}(1 - e^{-\left(\frac{z \cdot x}{\lambda}\right)}) \qquad \text{(Eqn. S1)}$$

$$I_d = I \cdot e^{-\left(\frac{d}{\lambda}\right)} \qquad \text{(Eqn. S2)}$$

$$I_{saturation} = I_{monolayer} \cdot \sum_{x=1}^{\infty} e^{-\left(\frac{z \cdot x}{\lambda}\right)} = I_{monolayer} \int_0^{\infty} e^{-\left(\frac{z \cdot x}{\lambda}\right)} \cdot dx = I_{monolayer} \cdot \frac{\lambda}{z} \qquad \text{(Eqn. S3)}$$

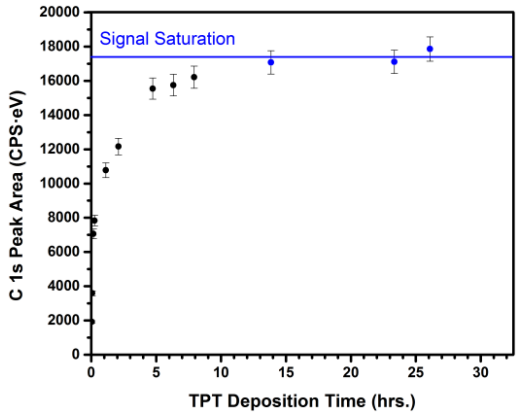

Figure S1. Plot of the XPS C 1*s* peak area of TPT on the Ag(111) surface plotted against the total deposition time of TPT to the surface.

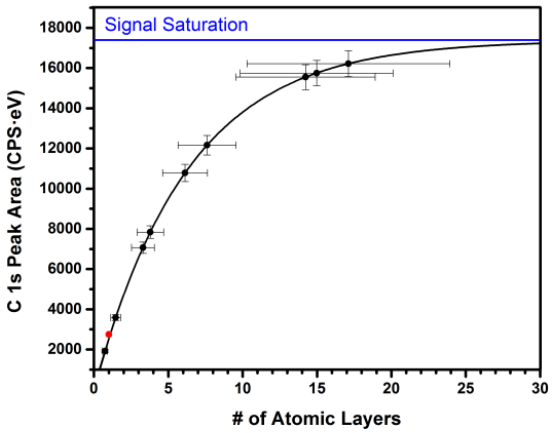

Figure S2. Plot of the XPS C 1*s* peak area vs the number of atomic layers of TPT on the Ag(111) surface. C 1*s* peak areas are quantitatively determined from XPS experiments. The red dot is the signal intensity corresponding to a 1.0 ML coverage.

Section S4. Thermal Desorption of the TPT Multilayer

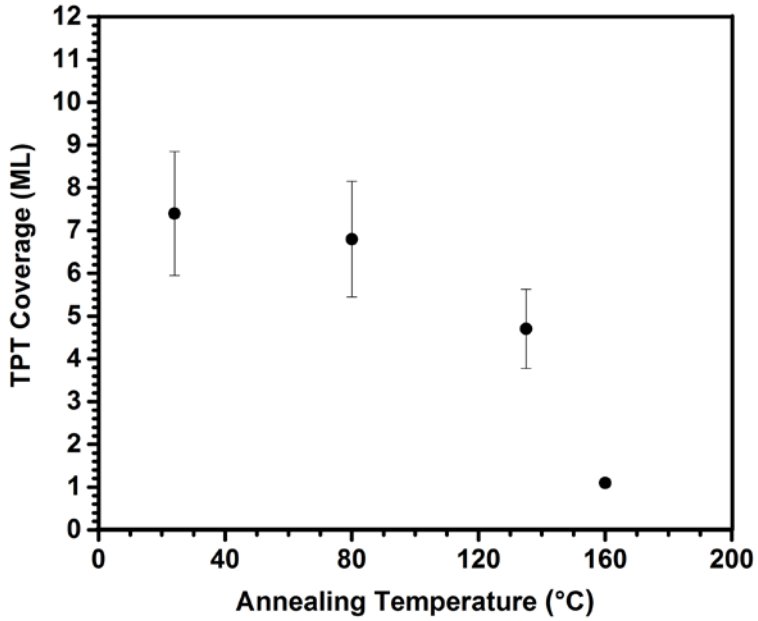

Figure S3. Plot of the TPT surface coverage vs the sample annealing temperature on the Ag(111) surface. To a sample with an initial TPT surface coverage of 6.5 ± 1.5 ML (C 1*s* peak area: 11,200 CPS·eV) annealing treatments at 80 °C, 135 °C, and 160 °C were consecutively applied, yielding coverages of 6.1 ± 1.4 ML (10,800 CPS·eV), 4.3 ± 0.9 ML (8,600 CPS·eV), and 1.0 ML (2,740 CPS·eV), respectively. Each annealing step lasted ca. 30 min and was followed by the gradual cooling of the sample at a rate of 0.1 °C/min. After the 160 °C anneal, the ordered TPT monolayer remained on the surface (identical to the structure in Figure 1a), as confirmed by STM image analysis.

Section S5. Additional XPS spectra of the TPT films on the Ag(111) surface

XPS N 1*s* data of TPT on the Ag(111) surface, acquired with surface coverages of 1.0 ML and 14 ± 4 ML, are shown in Figure S4. The 0.3 eV binding energy shift between these spectra indicates charge transfer from the Ag(111) surface upon TPT adsorption.[9] The N 1*s* peak position was found to be the same for all multilayer coverages studied (from a few ML to > 20 ML). The Ag $3d_{5/2}$ peak position did not differ between the experiments (368.3 eV). Effects of surface charging were not observed, presumably due to the conductive nature of the organic film.

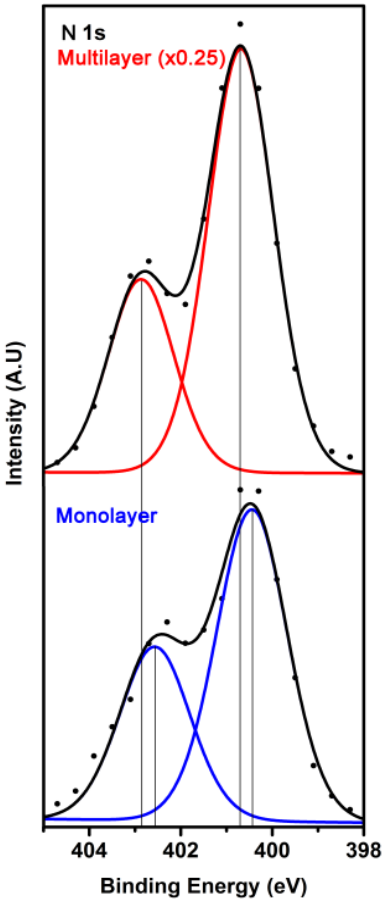

Figure S4. N 1*s* spectra for the multilayer (top) and monolayer (bottom) of TPT. Top: Organic multilayer spectrum acquired with a 14 ± 4 ML coverage, after subtraction of the spectrum corresponding to a coverage of 1.0 ML on the Ag(111) surface. N 1*s* peak positions are 400.7 eV and 402.8 eV. Bottom: Organic monolayer spectrum acquired with a 1.0 ML TPT coverage, after subtraction of the spectrum corresponding to atomically clean Ag. N 1*s* peak positions are 400.4 eV and 402.5 eV.

Section S6. Additional scanning probe images and line profiles of TPT films on the Ag(111) surface

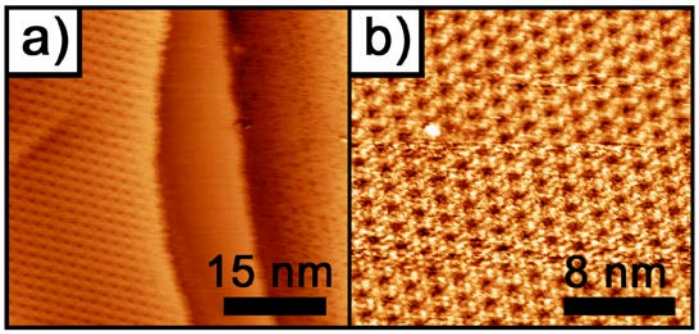

Figure S5. (a) STM wide image, and (b) zoom-in image of the porous, *sub-monolayer* phase of TPT on the Ag(111) surface. This structure only forms for low coverages of TPT, and has a two-dimensional packing density that is about half that of the full layer shown in Figure 1a. Image quality is low due to the low stability of the structure and mobile molecules on the surface, as seen on the right side of image (a). Note that this structure transitions to the structure shown in Figure 1a as coverage increases, therefore this structure is not present under the TPT multilayer, but rather the structure shown in Figure 1a. Also note that the less-dense layer shown here is not observed to form in the second layer or higher layers (see Figures 1c-1f and 4), but rather the packing of those layers is strongly directed by the stacking interactions to the dense close-packed phase of the completed first layer (Figure 1a).

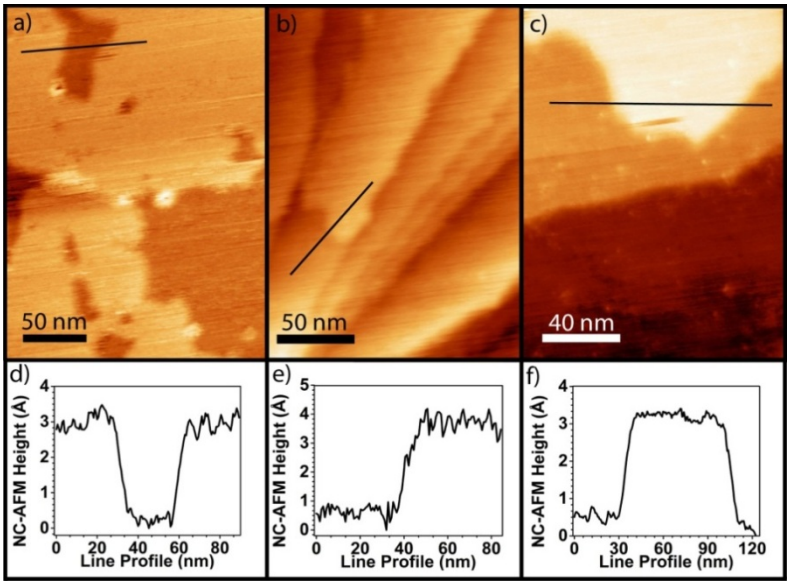

Figure S6. NC-AFM images of TPT on the Ag(111) surface with surface coverages of (a) 1.4 ML, (b) 6.1 ± 1.4 ML (annealed at 80 °C for 20 min.), and (c) > 20 ML. (d-f) Line profiles along the black lines in *a-c*. The height difference between the organic layers is measured to be 3.2 ± 0.2 Å by NC-AFM.

Section S7. Additional scanning probe images of TPT films on the reconstructed Au(100) surface

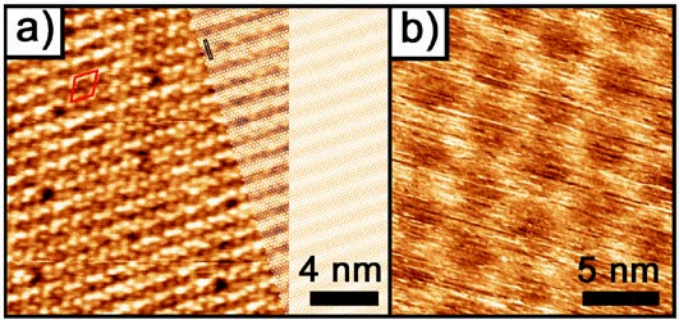

Figure S7. (a) STM and (b) NC-AFM images of monolayer TPT on the reconstructed Au(100) surface. The Au(100) surface has a c(26x68) reconstruction,[10, 11] illustrated to the right in (a), which is a nearly-hexagonal packing of surface atoms that have a very slight rumpling of the surface with a periodicity of 1.4 nm. That periodicity appears in the STM image of the monolayer, as shown to the left and in the overlay. The TPT unit cell is indicated by the red box, and the Au(100) surface reconstruction unit cell by the black box.

Section S8. Characterization of the electronic states of the TPT monolayer and multilayer films

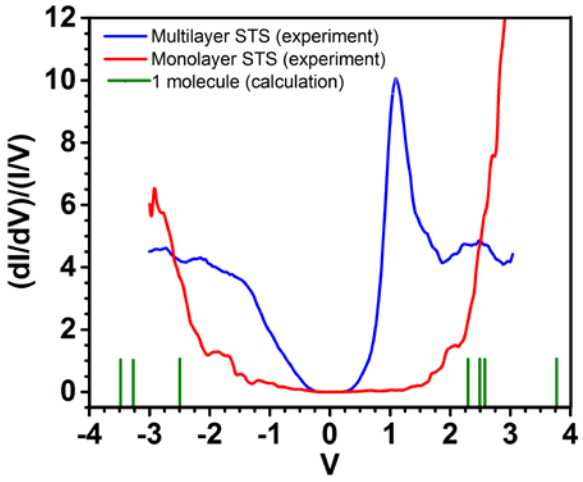

Figure S8. Scanning tunneling spectra (STS) of monolayer (red) and multilayer (blue) TPT films on the Ag(111) surface compared to calculated molecular orbital energies (green bars). Intensity at negative (positive) sample biases to the left (right) correspond to occupied (empty) electronic states. Scanning tunneling spectrum for the TPT monolayer that had been deposited with the sample heated at 50 °C during deposition (red line) shows a band gap ~4 eV, which is consistent with calculated molecular energy levels (green). Calculations (M06 / 6-31++G, Spartan) run to determine the HOMO – LUMO gap for a single TPT molecule in vacuum (green bars) yield a gap of 4.80 eV. STS for a TPT multilayer film that had been annealed at 50 °C for 15 min (8.8 ± 2.0 ML) (blue line) shows a band gap of *ca.* 2 eV. The asymmetry in the spectral features (large sharp peak at ~+1.1 V) may be related to the molecule being more prone to reduction than oxidation.

To characterize the electronic density of states, scanning tunneling spectroscopy (STS) measurements were conducted on the TPT monolayer and multilayer films at room temperature. Electrochemically-etched tungsten STM tips were conditioned on an atomically clean copper (100) surface and cleaned with an electron-beam tip heating module (RHK Technology) prior to each experiment. The STS measurements of the samples were acquired with the STM tip in quantum tunneling range by sweeping from negative sample bias voltages (corresponding to occupied states in the sample) to positive sample bias voltages (corresponding to un-occupied states in the sample). STS spectra were acquired initially over the voltage range from -0.5 to +0.5 V. Then, further STS spectra were acquired over incrementally increased voltage ranges (1 V range increase at each experimental step), up to a voltage range of 6 V (-3 to +3 V). Spectra acquired first with lower voltages were compared to those acquired later with higher

voltages to verify that the measured electronic density of states did not change with the application of higher voltages. STM imaging was also used to verify that the voltage sweeps did not damage the sample. Sets of STS spectra that changed in shape as the voltage range was incrementally increased in this way were assumed to have been affected by a change in the tip termination (adsorption of molecules onto the tip) and were therefore not included in the data analysis.

While varying the voltage bias, the tip-sample separation was simultaneously altered. The tip was displaced linearly in the direction normal to the sample with changes in the voltage. The tip moved 0.6 nm closer to the sample over the range from the minimum negative voltage to 0 V, and then 0.6 nm away from the sample over the range from 0 V to the maximum positive voltage. Then, the ratio of dI/dV to I/V was plotted versus the voltage. The aforementioned method for the STS data collection is described in detail elsewhere and is understood to provide a measure of the electronic density of states that is approximately independent of the tip-sample separation.[12] Experiments were conducted at room temperature; due to sample drift and the time required to record the data, the spectra should be considered as a spatial average over the molecule.

The monolayer was deposited with the sample held at 50 °C during the deposition and the corresponding STS spectrum is shown by the red line. The red line is an average of measurements from 8 sets of STS experiments acquired in different locations on the monolayer sample, each composed of 12 consecutive scans in the same location; *i.e.*, an average of 96 scans overall. The blue line is an average of a single STS experiment composed of 24 scans on a multilayer film with a surface coverage of 8.8 ± 2.0 ML, which had been annealed at 50 °C for 15 min before the STS acquisition. Numerous other data sets were acquired for the multilayer at the same or similar surface coverages that show similar features. The data shown is used because it is representative of those other experiments and composed of scans exhibiting the highest spectral resolution.

Calculations (M06 / 6-31++G, Spartan) were conducted to calculate the HOMO – LUMO gap for a single TPT molecule (green lines). Those calculations yield a gap of 4.80 eV. The band gap of the multilayer (< 2 eV, from STS experiment) is markedly smaller than the band gap of the monolayer (> 2 eV, from STS experiment) and a single molecule (4.80 eV, from DFT computation). We note that it is an understood phenomenon that the band gap for a multilayer film partaking in intimate π–π stacking will be significantly lower than the monomer[13] and that this is further evidence of molecular stacking and electron delocalization and transport in the layer.

Section S9. References

(1) Muzik, F.; Allan, Z. J. Aromaticke Diazoslouceniny XI. Kopulace se sym-Triaminobenzenem (Aromatic Diazo Compounds XI. Coupling with 1,3,5-Triaminobenzene). *Chem. Listy* **1952,** *46*, 774-775.

(2) Stepanow, S.; Strunskus, T.; Lingenfelder, M.; Dmitriev, A.; Spillmann, H.; Lin, N.; Barth, J. V.; Wöll, C.; Kern, K. Deprotonation-Driven Phase Transformations in Terephthalic Acid Self-Assembly on Cu(100). *J. Phys. Chem. B* **2004,** *108*, 19392-19397.

(3) Horcas, I.; Fernández, R.; Gómez-Rodriguez, J. M.; Colchero, J.; Gómez-Herrero, J.; Baro, A. M. WSXM: A Software for Scanning Probe Microscopy and a Tool for Nanotechnology. *Rev. Sci. Instr.* **2007,** *78*, 013705.

(4) Moulder, J. F.; Chastain, J. *Handbook of X-ray Photoelectron Spectroscopy : A Reference Book of Standard Spectra for Identification and Interpretation of XPS data*. Physical Electronics Division, Perkin-Elmer Corp.: Eden Prairie, Minn., 1992.

(5) Vickerman, J. C.; Gilmore, I. S. *Surface Analysis : The Principal Techniques*. 2nd ed.; Wiley: Chichester, U.K., 2009.

(6) Tait, S. L.; Wang, Y.; Costantini, G.; Lin, N.; Baraldi, A.; Esch, F.; Petaccia, L.; Lizzit, S.; Kern, K. Metal-Organic Coordination Interactions in Fe-Terephthalic Acid Networks on Cu(100). *J. Am. Chem. Soc.* **2008,** *130*, 2108-2113.

(7) Lingenfelder, M. A.; Spillmann, H.; Dmitriev, A.; Stepanow, S.; Lin, N.; Barth, J. V.; Kern, K. Towards Surface-Supported Supramolecular Architectures: Tailored Coordination Assembly of 1,4-Benzenedicarboxylate and Fe on Cu(100). *Chem.-Eur. J.* **2004,** *10*, 1913-1919.

(8) Ge, Y.; Adler, H.; Theertham, A.; Kesmodel, L. L.; Tait, S. L. Adsorption and Bonding of First Layer and Bi-layer Terephthalic Acid on the Cu(100) Surface by High-Resolution Electron Energy Loss Spectroscopy. *Langmuir* **2010,** *26*, 16325-16329.

(9) Tseng, T. C.; Urban, C.; Wang, Y.; Otero, R.; Tait, S. L.; Alcamí, M.; Écija, D.; Trelka, M.; Gallego, J. M.; Lin, N.; Konuma, M.; Starke, U.; Nefedov, A.; Langner, A.; Wöll, C.; Herranz, M. A.; Martín, F.; Martín, N.; Kern, K.; Miranda, R. Charge-Transfer-Induced Structural Rearrangements at Both Sides of Organic/Metal Interfaces. *Nature Chem.* **2010,** *2*, 374-379.

(10) Van Hove, M. A.; Koestner, R. J.; Stair, P. C.; Biberian, J. P.; Kesmodel, L. L.; Bartoš, I.; Somorjai, G. A. The Surface Reconstructions of the (100) Crystal Faces of Iridium, Platinum and Gold: I. Experimental Observations and Possible Structural Models. *Surf. Sci.* **1981,** *103*, 189-217.

(11) Van Hove, M. A.; Koestner, R. J.; Stair, P. C.; Biberian, J. P.; Kesmodel, L. L.; Bartoš, I.; Somorjai, G. A. The Surface Reconstructions of the (100) Crystal Faces of Iridium, Platinum and Gold: II. Structural Determination by LEED Intensity Analysis. *Surf. Sci.* **1981,** *103*, 218-238.

(12) Mårtensson, P.; Feenstra, R. M. Geometric and Electronic-Structure of Antimony on the GaAs(110) Surface Studied by Scanning Tunneling Microscopy. *Phys. Rev. B.* **1989,** *39*, 7744-7753.

(13) Gesquière, A.; De Feyter, S.; De Schryver, F. C.; Schoonbeek, F.; van Esch, J.; Kellogg, R. M.; Feringa, B. L. Supramolecular π-stacked Assemblies of Bis(urea)-Substituted Thiophene Derivatives and their Electronic Properties Probed with Scanning Tunneling Microscopy and Scanning Tunneling Spectroscopy. *Nano Lett.* **2001,** *1*, 201-206.